Experiments in Fluids (2021) 62:132
https://doi.org/10.1007/s00348-021-03226-3

RESEARCH ARTICLE

Voltage rise anemometry in turbulent flows applied to internal combustion engines

Michael Wörner[1] · **Gregor Rottenkolber**[1]

Received: 17 February 2021 / Revised: 7 April 2021 / Accepted: 10 May 2021 / Published online: 30 May 2021

Abstract

In an experimental procedure, a voltage rise anemometry is developed as a measurement technique for turbulent flows. Initially, fundamental investigations on a specific wind tunnel were performed for basic understanding and calibration purpose. Thus, a mathematical correlation is derived for calculating flow from measured secondary voltage of an ignition system under different thermodynamic conditions. Subsequently, the derived method was applied on a spark-ignited engine to measure in-cylinder flow. Therefore, no changes on combustion chamber were necessary avoiding any interferences of the examined flow field. Comparing four different engine configurations, a study of mean flow and turbulence was performed. Moreover, the results show a clear correlation between measured turbulence and analysed combustion parameters.

Graphic abstract

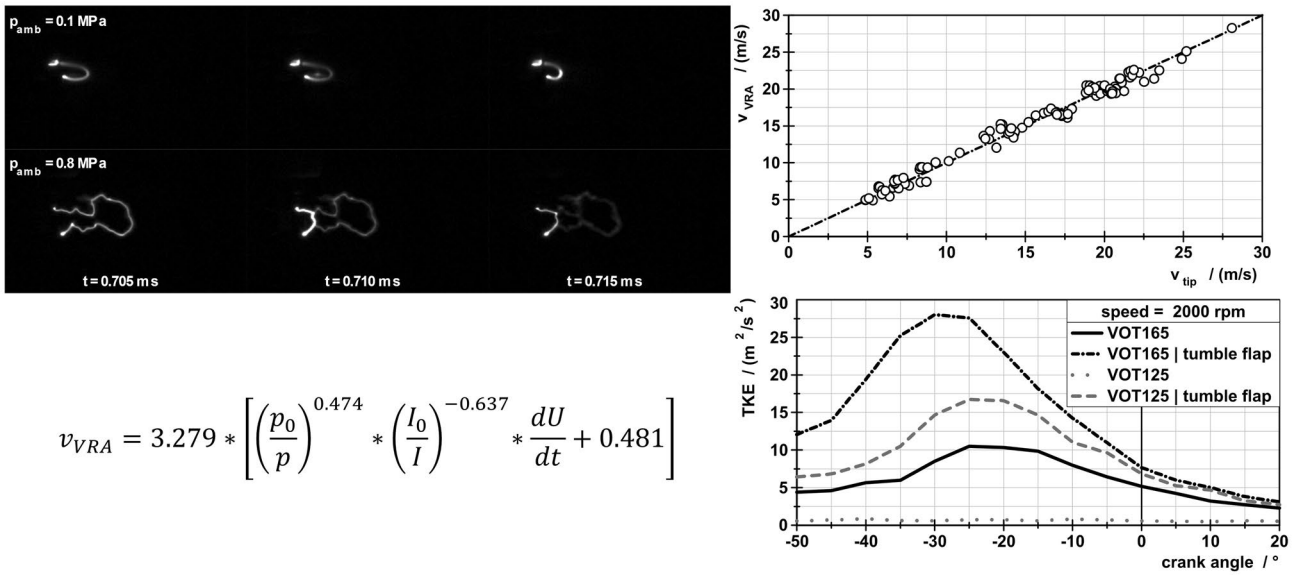

$$v_{VRA} = 3.279 * \left[\left(\frac{p_0}{p} \right)^{0.474} * \left(\frac{l_0}{l} \right)^{-0.637} * \frac{dU}{dt} + 0.481 \right]$$

1 Introduction

In-cylinder flow has an important influence on the quality of combustion process of internal combustion engines (ICE). In spark-ignited (SI) engines, different modes of action have an impact.

Firstly, charge motion improves mixture preparation. Especially reproducible local conditions at spark plug are essential

✉ Michael Wörner
michael.woerner@hs-esslingen.de

[1] Automotive Powertrain Laboratory, Faculty of Mobility and Technology, Esslingen University of Applied Sciences, Kanalstr. 33, 73728 Esslingen, Germany

for a robust inflammation. Besides high turbulence levels, low cycle-to-cycle variations are essential (Fischer 2004).

Secondly, there is a great impact of the turbulence level on burning speed. In homogenous premixed SI engines, turbulent flame speed depends massively on the turbulence level of the flow (Merker and Teichmann 2018). However, the tumble type of charge motion has become well established for SI engines. At the end of compression, the decay process of the tumble flow leads to an increase of turbulent kinetic energy (TKE). This effect supports flame kernel growing right after ignition as well as a fast burn-through of the whole charge (Riess et al. 2013; Merker and Teichmann 2018).

Concepts with an early intake valve closing (EIVC) get more and more established in modern gasoline direct-injection (GDI) engines. This brings large benefits due to dethrottling at part load and lower knock tendency at high load due to reduced effective compression, which is well-known as the Miller-Cycle (Merker and Teichmann 2018). However, a major drawback of this EIVC strategy is the reduced charge motion (Riess et al. 2013). Detailed knowledge about in-cylinder flow turbulence is essential to improve those concepts, and also in general for further engine development.

The voltage rise anemometry (VRA), which has not been established as a measurement technique for ICE until today, could be an appropriate method for in-cylinder turbulence measurement. Lindvall (1934) already mentioned the method in the 1940s. He compared VRA to hot wire anemometry (HWA). Later some further investigations were performed (Schaudt et al. 1985; Gardiner et al. 2008; Kim and Anderson 1995; Pashley et al. 2000; Paa, 2019). Especially, the research project of Schaudt et al. (1985) extended the expertise. By varying thermodynamic conditions as well as using different gases they found out different dependencies.

In this study, the authors also did some basic studies on the VRA in a wind tunnel and largely confirmed the findings of Schaudt et al. (1985). Moreover, mathematical correlations for calculating flow velocity from the voltage drop of the ignition system were derived. Furthermore, using appropriate statistics, flow velocities and even TKE of different types of charge motion inside the combustion chamber of a direct-injection spark-ignited (DISI) engine could be measured for the first time via VRA. To confirm the applicability of the novel measurement approach, mean flow and turbulence were correlated to combustion performance.

2 Physics and theoretical overview

2.1 Function principle of the VRA

Fundamentally, voltage rise anemometry bases on the measurement of the voltage of a generated plasma channel for local flow analysis. Using a SI engine, the standard spark plug is suitable to generate the plasma. Hence, as a very big advantage, no changes on the combustion chamber are necessary. Additionally, the investigation of the flow takes place directly at the spark plug, which is the area of highest importance for the SI combustion process (Günther et al. 2013).

In general, two physical effects of a glow discharge are essential for the VRA.

Firstly, the generated plasma channel follows the prevailing flow, which leads to a stretching of the channel. The quick response of the ionized particles of the plasma enable even an immediate response on strong fluctuations of the flow (Lindvall 1934). This is a key factor of VRA for successful measurements in turbulent flows.

Secondly, the elongation of the spark results in an increase of its resistance. This in turn leads to a second physical effect. The measured voltage across the electrodes of the plasma generator (e.g. spark plug electrodes) increases with the length of the discharge channel due to the increase of resistance. Correlation of plasma channel length and voltage drop can be found in Paa (2019), Sandhu et al. (2019), Shiraishi et al. (2016) and Tilz et al. (2019) and is defined as:

$$v \sim \frac{dL_{\text{plasma}}}{dt} \sim \frac{dU_{\text{plasma}}}{dt}. \tag{1}$$

If the plasma channel achieves a certain length, a restrike occurs. In this case an energetic favourable way exists on a shorter path length, which is later on a subject of discussion in Sect. 4.1. This shortened channel shows lower resistance again and the voltage decreases rapidly.

Figure 1 illustrates the described elongation of a spark by constant orthogonal flow. As one can see, the relation between flow and change of elongation differs in dependence of the present state of deflection. First after breakdown (t0), there is a lower deflection. Once the flow moves

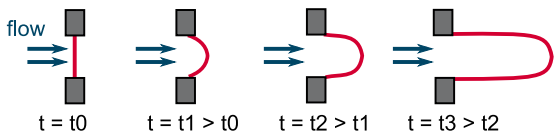

Fig. 1 Schematic spark deflection at constant homogenous flow orthogonal to the electrodes

the spark away from the electrodes and shapes the tip of the channel, a clear correlation of spark stretching and flow is accessible. The change from time step t2 to t3 illustrates this behaviour. The flow only stretches the upper and lower part of the channel, which leads to a relation of 0.5 roughly (Schaudt et al. 1985).

For evaluating spark deflection, whether optically or by measuring voltage change, it is necessary to use only time periods where spark deflection has reached a certain threshold. Thus, a reliable interpretation of flow velocity is possible.

As mentioned, there is a clear relation of discharge channel length and voltage drop across the electrodes. However, there are more parameters, which affect the value of the voltage drop. If the electrical current of the plasma channel decreases, the cross section of the channel gets smaller. By this, surface to volume ratio decreases and thermal convection from channel to ambient rises. The resulting lower channel temperature leads to a lower conductivity. To sustain the channel, a stronger electric field is required resulting in a stronger voltage drop (Schaudt et al. 1985; Schneider et al. 2016; Küchler 2017).

Another influencing parameter is the change of ambient pressure. Pressure rise causes a higher charge carrier concentration which leads to a smaller cross section of the channel keeping the current constant. Again, this results in a lower channel temperature due to higher thermal losses. The conductivity decreases and a stronger voltage drop can be observed (Schaudt et al. 1985). As well, using different types of gas the level of voltage drop changes due to different densities of charge carriers.

In case of varying ambient temperature, no changes in voltage drop could be determined. Due to high temperatures of a glow discharge, ambient temperature does not affect the density of the plasma channel, and therefore, charge carrier density and movement are not influenced (Schaudt et al. 1985; Küchler 2017).

Using a standard spark plug with one ground electrode (hook shape), the orientation of the ground electrode has to be respected. The adjustment should be more or less orthogonal to the cross flow. For an upstream position of the ground electrode, areas of slipstream can distort the measurement results. For a downstream position of the electrode, the flow blows the spark straight to the electrode and cannot elongate further (Günther et al. 2013; Zadeh et al. 2019).

Generally, all the known publications on the VRA had to deal with some impairments. In particular there is to mention the use of standard inductive ignition systems. This leads to a short spark duration and a strong dropping current profile during the discharge (Kim and Anderson 1995; Pashley et al. 2000; Sandhu et al. 2019). Furthermore, many researchers could not apply statistically based post-processing and could not extract the assessable sections of the signal (Gardiner et al. 2008). Finally, in the past the focus was never on measuring turbulent kinetic energy.

2.2 In-cylinder charge motion

The description of turbulent flow usually follows the definition of Reynolds, which separates the flow in a mean and a fluctuation velocity. Still, there is a separation depending on the behaviour of the mean value, which can be constant or time depending. This in turn leads to different ways of calculation. The constant mean flow allows time averaged solutions. In case of transient mean flow an ensemble averaged method has to be applied. This usually leads to a high number of required measurement data. Anyway, in case of in-cylinder flow of internal combustion engines constant mean flow is never prevailing. Thus, mean velocity and fluctuation velocity are always a function of time.

However, in case of cyclical repetition of the flow, as it occurs in internal combustion engines, this kind of consideration still leads to an error. Transient flow conditions during the intake stroke lead to conditions in the compression stroke, which can differ from cycle to cycle. In consequence the mean velocity of the flow varies from cycle to cycle. Hence, the consideration of those cyclic variations is also essential for detailed calculation of turbulent fluctuations (Lancaster 1976; Heywood 1988; Stone 1999).

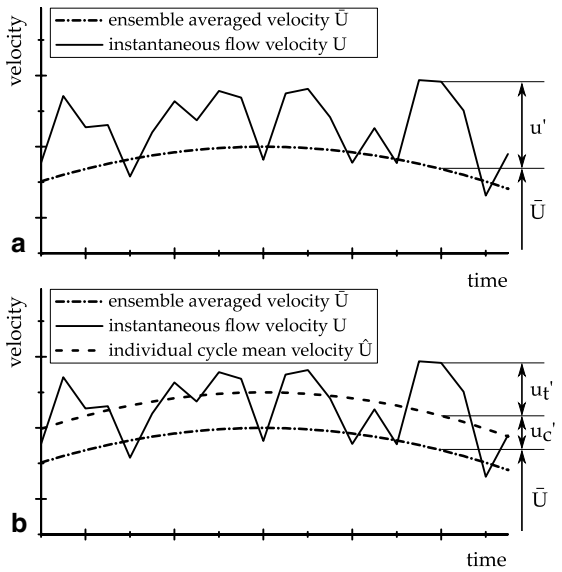

Fig. 2 Two different approaches to define turbulent flow: **a** definition of Reynolds with an averaged velocity Ū and a fluctuation velocity u'; **b** definition of turbulent flow by ensemble averaged velocity Ū and a cyclic and turbulent fluctuation velocity u_c' and u_t' (based on Fischer (2004))

Figure 2 illustrates the both mentioned approaches. In both diagrams, the solid line is the same instantaneous flow velocity. In case of a combustion engine, it represents the flow of one cycle. The dash-dotted line is the ensemble averaged mean velocity of a certain number of cycles. In the bottom diagram, additionally the mean velocity of the individual considered cycle is shown. By this, Eq. (2) comes up, where *i* describes the cycle number. Neglecting the cyclic fluctuation speed u_c' results in an overestimation of the turbulent fluctuation u_t' (in the top diagram u' is the only fluctuation speed, which in this case describes turbulence). This error gets even worse in case of investigating and comparing configurations that may cause a different level of cyclical fluctuations of the flow.

$$U(t,i) = \overline{U}(t) + u_c'(t,i) + u_t'(t,i). \tag{2}$$

3 Experimental setup

3.1 Flow test rig and measurement technique

The small wind tunnel shown in Fig. 3 allowed fundamental research work. The pipe has an inside diameter of 36 mm and can be pressurized up to 4 MPa. Operation is possible with different gases. So far, air and nitrogen were used. The impeller *I* allows flow velocities up to 40 m/s and the heater *II* can heat up the gas up to 473 K. A thermal mass flow meter *III* enables the measurement of the gas velocity in the test rig as a reference value. The position *IV* represents the integrated ignition chamber. In this volume, the installed series spark plug of the used SI engine generated the arc for the investigations. Additionally, there are two glass windows *V* in the chamber. This allowed optical observation of the deflection of the plasma channel.

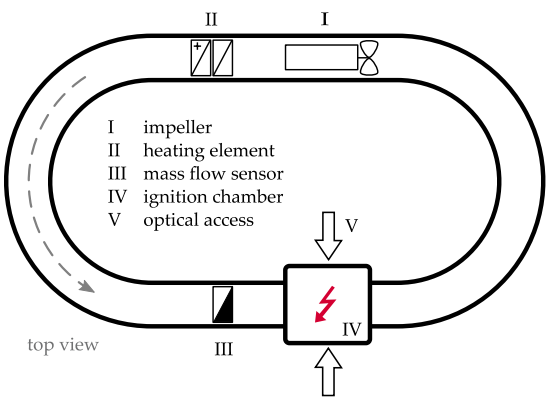

Fig. 3 Flow test rig (schematic drawing) for basic VRA investigation

To pave the way for detailed research on VRA, the use of an ignition system with constant current was more or less necessary. The used system includes a standard ignition coil combined with a step-up converter. The inductive system performs the breakdown voltage, whereas the converter enables an extension of the discharge duration; see Brandt et al. (2017). Thus, a longer measurement duration was possible which resulted in higher quantity of data and therefore higher accuracy. Figure 4 shows current profiles for three different power levels of the ignition system. In this case, maximum time duration of the spark phase was applied without cross flow.

The setting of a high voltage probe (Tektronix P6015A) and an optical current sensor (FOS OCS 1000) between coil and spark plug allowed measurement of secondary parameters of the ignition system. For recording those signals together with trigger, an oscilloscope (Yokogawa DLM4038) with a sampling rate of 1.25 MS/s was used. At measurements on the flow test rig, 20 ignition events per measurement point were recorded. For studies on the engine test bench, a higher value of 250 ignition events was sampled due to transient flow conditions.

The used high-speed camera for optical flow measurements was a Photron FASTCAM SA-X2. Frame rate was 200,000 f/s at a resolution of 256 × 152 px and an exposure time of 1/295890 s. For observing the spark deflection, the area of interest was around 17 × 10 mm. For optical evaluation, ten ignition events per measurement point were recorded.

3.2 Test engine

The research engine was a GDI single cylinder test engine. It bases on the Mercedes-Benz mass-production engine M 274. This GDI engine has a centre mounted injector and a spark plug positioned between the exhaust valves. Figure 5 shows a schematic drawing. This figure as well includes the used charge motion system. The black line in the inlet port demonstrates a tumble flap, which could optionally be installed. The installation blocked half cross section of

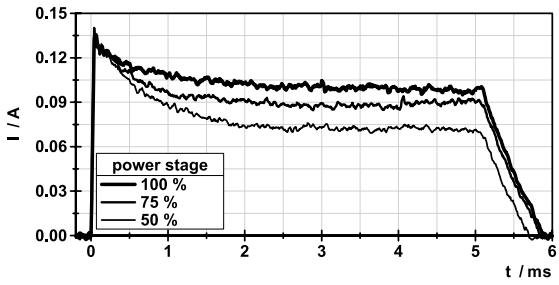

Fig. 4 Current profiles for the three power stages of the ignition system without any cross flow

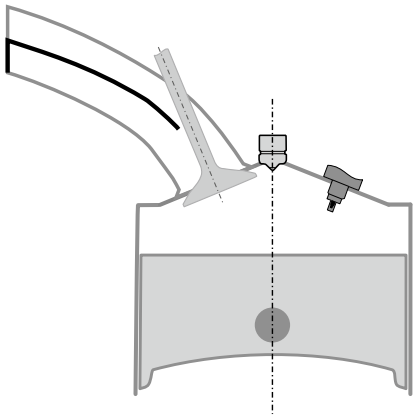

Fig. 5 Research engine combustion chamber with centre mounted injector and spark plug between exhaust valves (schematic drawing); the black line in the intake port marks the tumble flap which can be installed

Table 1 Research engine parameters

Type	Single cylinder
Displacement [cm^3]	497.8
Stroke [mm]	92
Bore [mm]	83
Connecting rod length [mm]	138.7
Compression ratio [-]	13.6: 1
Inlet valve diameter [mm]	30.5
Exhaust valve diameter [mm]	24.0
Valves per cylinder [-]	4
Charge motion system	Tumble flap

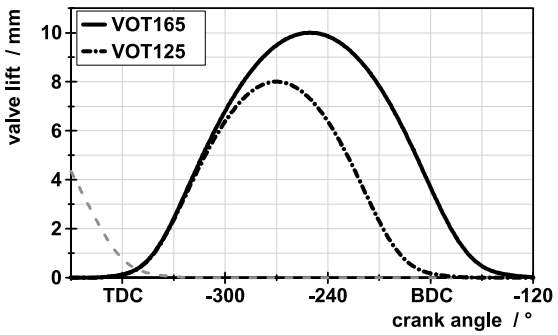

Fig. 6 Inlet valve lift profiles: Standard profile with valve opening time (VOT) of 165°CA at 2 mm valve lift (solid line) and EIVC profile with VOT of 125°CA at 2 mm valve lift (dash dotted line); exhaust valve lift profile (dashed line)

the inlet port, which caused higher flow velocities. Further, Table 1 includes the most important data of the engine.

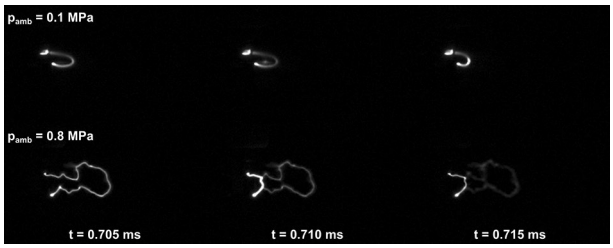

Fig. 7 Recorded frames of spark deflection at two different ambient pressures with a restrike event at the mid frame of each row; top: p_{amb} = 0.1 MPa; bottom: p_{amb} = 0.8 MPa

Figure 6 shows both used valve lift profiles. Designation number in VOT165 / VOT125 represents valve opening time (VOT) in crank angle degree (°CA) at 2 mm valve lift. The opening angle kept constant for all measurements. An important objective of the chosen opening angle was the prevention of internal residual gas due to valve overlap. Therefore, the dashed line illustrates the exhaust valve.

4 Methodology

The experimental procedure and applied methodologies can be divided into four sections. First, optical investigations of the spark deflection. Second, voltage signals analysis including the detection of restrike events and the approximation of voltage rise. Third, flow velocity calculation from voltage rise and calibration procedure. Finally, a statistical method for crank angle (CA) wise calculation of mean flow and turbulence at a motored combustion engine.

4.1 Optical analysis of the spark deflection

Optical spark investigation is indeed not necessary for the development of the VRA method. However, it supports greater understanding of signal characteristics. Figure 7 shows three frames for two different ambient pressures. In each case a restrike event occurs in the mid frame. The higher pressure leads to greater spark deflection and more wrinkling, which is in good accordance with open literature (Shiraishi et al. 2016; Zheng et al. 2018).

Further, by tracing ionized particles, a calculation of the prevailing flow was possible. This enabled a comparison between the flow downstream of the spark plug and the mass flow meter positioned upstream of the spark plug. Other authors like Gardiner et al. (2008) found considerable differences between incident flow velocity and the velocity at the tip of the spark.

In the following, two different methods for optical velocity calculation are described. The velocity, calculated from the movement of the tip position of the plasma channel,

named v_{tip}. Moreover, from the change of plasma length, the velocity v_{length} was determined. The calculated channel lengths were multiplied with the factor 0.5 (see Sect. 2.1).

For all optical evaluations, a specially programmed code in the software MATLAB was used. Figure 7 already showed recorded images as an example. The standard settings for the recordings are described in Sect. 3.1. In a first step, the electrodes were removed from the images. Further on, with a decent grey colour threshold, the sequences of images were transformed to binary images. Figure 8a shows an example of such an image. The grey surface illustrates the detected pixels of the elongated spark. From this point, it was possible to define the area of the spark by counting the pixels (Sandhu et al. 2019). As the images in Fig. 7 show, the brightness of the plasma channel depends on prevailing conditions and changes constantly. Therefore, it was almost impossible to calculate the channel area using a fixed threshold for binarization. Further, the varying channel thickness made a clear correlation between channel area and channel length difficult.

More accurate and evaluable was the detection of the forward position of the plasma channel. As one can see in Fig. 8b, from the changes of the tip position between the images, the velocity v_{tip} was calculated.

Subsequently regarding simplified evaluation, the plasma channel was divided into an upper and lower part at the tip positon. As shown in Fig. 8a with the black lines, two spline functions were calculated and simply added for the channel length. Of course, there was a small error around the tip position where the spline functions end. In case of an extreme wrinkling plasma channel the calculation could be even more defective. Therefore, incorrect channel length values, which showed clear unsteady behaviour, were rejected.

Figure 8b contains the spline curve and tip position of the discharge from Fig. 8a along with an earlier time step (dashed line). Differentiating those lengths and tip positions resulted in the two optical velocities v_{length} and v_{tip}.

Discrepancies among the two optical velocities occurred if the flow stretched the spark not only in flow direction but also vertically. In particular higher ambient pressure, where spark wrinkling increased (see Fig. 7), and higher flow speed intensified this effect. As one can see in Fig. 9, there was mostly a higher v_{length} (squares) than v_{tip} (triangles) determined. At low flow velocities v_{tip} and v_{length} reached similar levels. In case of calculating a velocity from the change of spark channel length, this confirmed the requirement of a variable factor depending on flow and thermodynamic conditions. As mentioned before, in this study it was kept constant at 0.5.

More important in terms of developing the VRA technique, was the fact that there seemed to be just a small deviation between incident flow and spark movement. In Fig. 9, the measured bulk flow (dots) was almost equal to v_{tip} (triangles).

Obviously, from a more detailed analysis of the optical investigations more scientific insights could be obtained. In fact, that was not the focus of the current work. For the validation of the working principal of VRA it was enough to determine a good matching between the elongation of the plasma channel and the bulk flow velocity.

4.2 Signal analysis and restrike detection

As explained in Sect. 2.1, the elongation of a discharge channel under continuous flow showed a characteristic voltage curve. The repetitive stretching and restrike events resulted in repetitive rises of the voltage followed by abrupt declines. The diagram of Fig. 10a illustrates

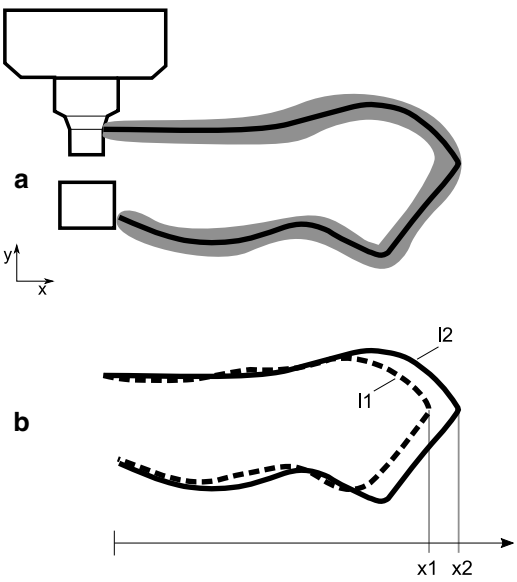

Fig. 8 **a** Results of optical evaluation process: plasma area after binarization (grey pixels); spline function of plasma channel length calculation (black line); **b** spline function and tip position of two time steps t1 and t2

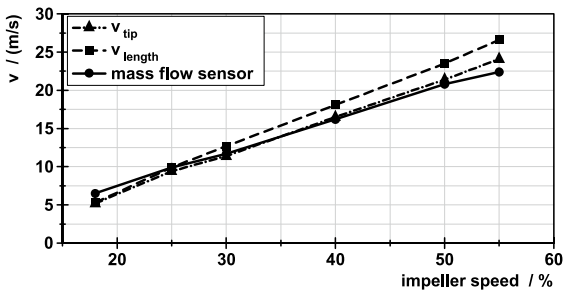

Fig. 9 Optical measured flow velocities v_{tip} (dash dotted line) and v_{length} (dashed line) compared to the velocity measured by the mass flow sensor (solid line) for different impeller speeds

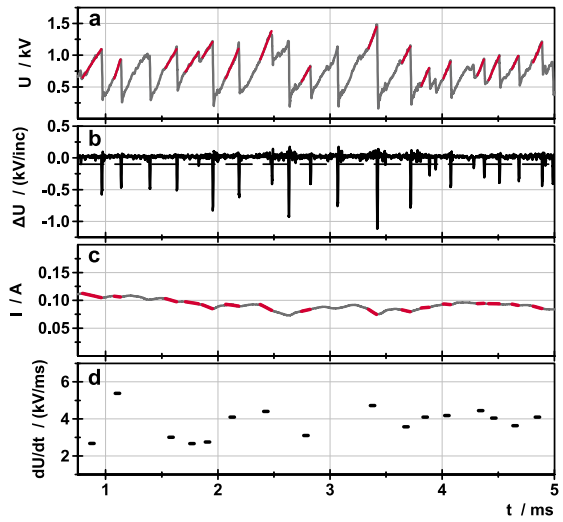

Fig. 10 **a** Measured voltage signal and evaluated gradients; **b** differentiated voltage signal for restrike detection with threshold (dashed line); **c** current signal with relevant areas marked; **d** resulting gradients dU/dt for the evaluated sections

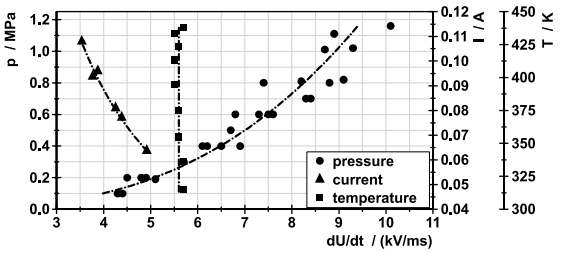

Fig. 11 Dependences of the voltage change dU/dt on pressure (dots), current (triangles) and temperature (squares)

such a curve of the voltage drop across the electrodes. However, the maximum voltage level and frequency of restrike events highly depended on thermodynamic and flow conditions. It is obvious that the phases of rising voltage were of special interest because they were the result of plasma stretching in flows. The rapid drop of voltage at plasma channel breakdown allowed a clear detection of restrike events. As clarified earlier in Sect. 2.1, the best correlation of spark deflection and flow velocity was expected at large deflections. Thus, evaluating the signal backwards of restrike, valid detection of the section of interest could be ensured.

The diagram of Fig. 10b shows the differentiated voltage signal. It illustrates the described phenomenon of clear restrike detection. Subsequent a linear approximation of the signal before the restrike was carried out. Therefore, an initial setting of several criterions was necessary to ensure a requested quality of evaluated deflections. With respect to the evaluation routine, there is to mention a threshold of a minimal voltage representing a minimal elongation and a second threshold for the minimal number of data points used for the approximation of the voltage rise. As well, minimal permitted determination of the approximation was required.

In Fig. 10a, the red lines define the evaluated approximations of this example voltage signal. In Fig. 10d, markers represent the resulting gradients, which were stored time synchronous.

Additional to this interim result, mean values and gradients of current, pressure and temperature were saved for every determined gradient. Figure 10c shows the related current signal of this measured discharge and the marked sections of the gradient analysis. Note that the noise of the shown signal was cancelled by a low pass filter.

Current profile evaluation at each section of gradient analysis was also used for error control. Setting limits for gradient and absolute value of the current signal, incorrect values (e.g. current drops to zero at short circuit condition) could be rejected.

4.3 Flow calculation

This section describes the further evaluation process as well as the calibration procedure. Therefore, as mentioned in Sect. 2.1, the investigation of the dependencies of voltage drop was necessary. Earlier mentioned literature describe potential correlations of voltage on pressure and current, which were basically used in this work as well, but modified and calibrated in a new way.

Measurements at different flow velocities and thermodynamic conditions were performed on the flow test rig. Additionally, the output power of the ignition system was varied to model different current levels. As an example, Fig. 11 shows measurement series of different variations. Note, the impeller speed of the test rig kept constant for each series, which realized nearly constant flow velocity. It is important to clarify that the gradient dU/dt in this figure is not the raw measured gradient. To display separated effects in this diagram each measuring was corrected by the other influences. Similar results compared to the mentioned literature (see Sect. 2.1) could be found. Increasing system pressure gradients became larger (dots), whereas an increasing current across the plasma channel reduced the gradients (triangles). Also in good agreement with literature, within the investigated temperature range no influence of ambient temperature could be determined (squares).

Equation (3) represents the resulting formula after calibration procedure. The exponents were determined by using a Least Squares Method. The reference values were chosen from measurement data to $p_0 = 2$ bar and $I_0 = 0.1$ A. Additionally, the equation includes the resulting linear relation between gradient dU/dt and flow velocity. Thus, implementing this equation in the evaluation process a direct flow

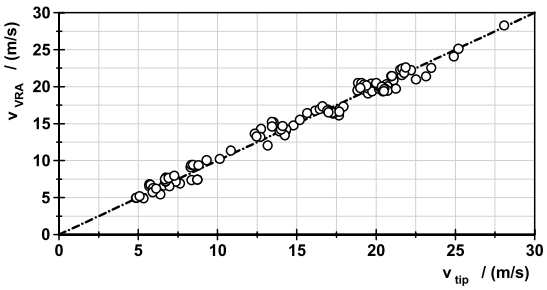

Fig. 12 Final results of the calibration process of the derived function

velocity calculation for each detected restrike event was possible.

$$v_{VRA} = 3.279 * \left[\left(\frac{p_0}{p} \right)^{0.474} * \left(\frac{I_0}{I} \right)^{-0.637} * \frac{dU}{dt} + 0.481 \right] \quad (3)$$

Figure 12 illustrates the final results of the calibration process of the VRA method on the flow test rig. Again, each of the 108 measurement points contained 20 ignition events leading to approximately 300 evaluated restrikes per measurement point. The optical velocity v_{tip} was identified as the most robust reference and hence used for calibration.

At the current stage of development process, there are few limitations of the formula which should be mentioned. As one can see, the maximum calibrated velocity was close to 30 m/s. The lower limit was at a flow velocity of 5 m/s. Further investigations for higher and lower flow velocities should be performed in the future. Unfortunately, the current experimental setup was limited and defined the calibration interval. Another limitation was the maximum pressure due to a restriction of the used ignition system. Hence, the accuracy of the calibration function remains valid up to about 1.2 MPa.

4.4 Crank angle based statistics

As already mentioned in Sect. 3.1, a higher quantity of 250 ignition events per measurement point was used for flow measurements in the combustion chamber of a SI engine. This value represented the recorded cycles. Figure 13 illustrates the established approach for calculating crank angle based flow information. Shifting the ignition timing led to the required high quantity of data per crank angle. Note, only the crank angle range at the end of compression around top dead centre (TDC), which is of interest for ignition and flame formation, was investigated. Moreover, the current work focused only on motored engine conditions without injection. The air mass flow was equal to an engine load of $IMEP_n = 3$ bar at engine speed of 2000 rpm and was kept

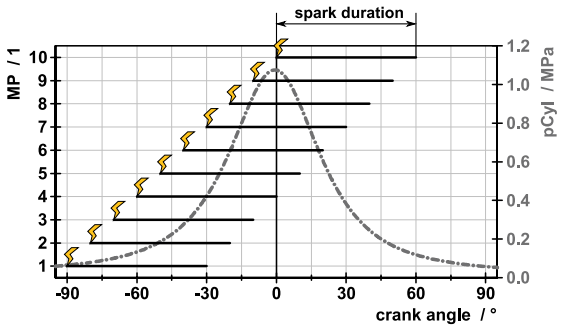

Fig. 13 Measurement principle for crank angle wise flow analysis with the VRA method; in-cylinder pressure signal (dash dotted line); spark duration of different measurement points (solid lines)

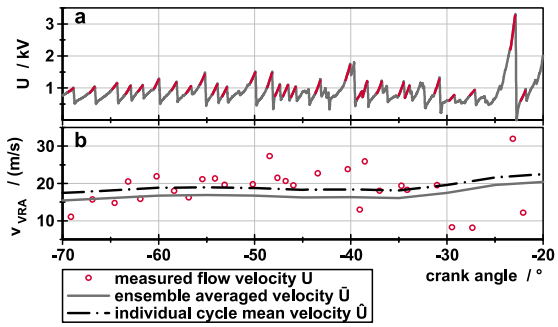

Fig. 14 **a** Measured voltage with evaluated gradients; **b** resulting velocities from the signal above (red dots), ensemble averaged velocity Ū (solid line) and individual mean velocity Û (dash dotted line)

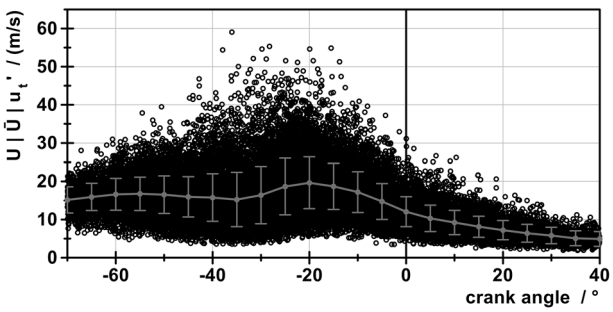

Fig. 15 Measurement example: VOT165 | tumble flap; resulting velocities (black dots); ensemble averaged velocity Ū (solid trace, grey dots); turbulent fluctuation velocity u_t ' (deviation bars)

constant for all displayed engine VRA measurements in this work.

Measured data were evaluated in four steps, starting with the detection of all evaluable spark deflections and the calculation of the respective velocities. Diagram a) of Fig. 14 shows again an example of a spark event as it is already known from flow test rig investigations. Diagram b shows the calculated flow velocities (red dots) over crank angle.

Additionally, Fig. 15 shows all analysed flow velocities of this configuration (black dots) including the example data of Fig. 14b as well.

Once this calculation was finished and all velocity data were linked to crank angle position, the second evaluation step started. For evaluating the ensemble averaged velocity $\bar{U}$ an allocation of data in windows of five crank angle degrees followed. The grey dots and grey line in Fig. 15 mark the result as well as the grey line in Fig. 14b. Obviously, the width of the chosen crank angle windows affected the results slightly. Nevertheless, by varying this value the authors determined five degrees as a good compromise between crank angle resolution and data number for adequate statistical power (minimum value of 1000 flow values per window).

Subsequently, evaluation procedure took up all spark events of each single cycle again. To evaluate the individual cycle mean velocity $\hat{U}$ (dash dotted line in Fig. 14b) the arithmetic mean of the relevant section of crank angle (here − 70 to − 20°CA after TDC) had to be calculated. The difference between each cycle mean value and the ensemble averaged mean value within this interval represented the individual cycle deviation which had to be added to the ensemble averaged trace to get the cycle individual mean velocity $\hat{U}$.

The resulting difference between each measured velocity (red dots in Fig. 14b and the individual cycle mean velocity $\hat{U}$ finally represented the most relevant turbulent fluctuation velocity u_t'. The difference between ensemble and time averaged values provided information about cyclic fluctuations (u_c').

Eq. (2) in Sect. 2.2 already showed the mathematical link of the three velocity components of the turbulent transient flow with cycle-to-cycle variations. Figure 15 contains all measured values (black dots), the ensemble averaged velocity (grey line) and the turbulent fluctuation speed u_t' (grey deviation bars) for one example setting.

Even though spark plug is mounted in a position where the ground electrode was orthogonal to expected bulk flow, variations of flow direction could lead to an error. In case of spark elongation in direction of the ground electrode, lower values may result. Nevertheless, due to high statistical power of numerous data the authors expect sufficient accuracy.

5 Engine test results

The developed method was first validated with crank angle wise measurements in motored engine operation. Therefore, the inlet configuration of the engine was varied. Each engine setup was investigated with the described method of Sect. 0. In a second step, motored operation for VRA measurements and fired operation for combustion analysis were performed.

5.1 VRA under different in-cylinder flow conditions

The effects of different engine setups on the local flow at spark plug were investigated. For comparisons, average flow velocity $\bar{U}$ was considered first. Furthermore, turbulent kinetic energy was calculated by Eq. (4). Using the turbulent fluctuation u_t' from the VRA method provided direct information about the local level of turbulence around spark plug.

$$TKE = 0.5 * u_t'^2 \tag{4}$$

Figure 16 contains the results of four different setups. The big valve lift profile with the tumble flap (dash dotted line) resulted in highest flow intensities. The EIVC configuration (dotted line) led to a decrease of velocities compared to the standard configuration (solid line). EIVC in combination with the tumble flap (dashed line) led to an increase of charge motion. The results of the mean flow velocity $\bar{U}$ in diagram a) confirmed results of open literature (Ogink and Babajimopoulos 2016; Merker and Teichmann 2018).

As one can see, VOT125 configuration (dotted line) behaved completely different to the other three and did not show any change over crank angle. It seems like there was almost no measurable spark deflection and hence, no measurable air flow. This measurement confirmed the extreme reduction of in-cylinder charge motion with an EIVC strategy; see also Scheidt et al. (2014) or Riess et al. (2013).

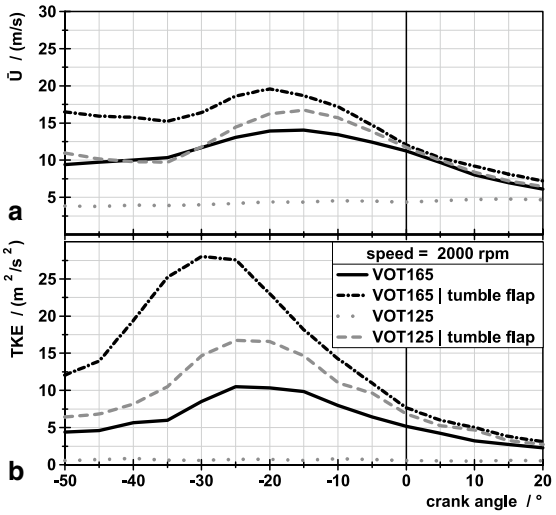

Fig. 16 Results of the VRA measurements for four different inlet configurations: VOT165 (solid line), VOT165 with tumble flap (dash dotted line), VOT125 (dotted line) and VOT125 with tumble flap (dashed line); **a** ensemble averaged velocity $\bar{U}$; **b** turbulent kinetic energy

In general, magnitude and trend of the graphs assigned to the specific intake configurations were comparable to results of other measurement and simulation results of before mentioned literature. Except the VOT125 configuration, there was an increase of the mean flow velocity during compression up to a certain crank angle detectable. Later in the compression stroke dissipation processes of the main vortex occurred and the mean flow velocity mitigated. Once the piston passed TDC the differences between mean flow velocities of the three configurations were marginal.

Note, the measured values are local flow velocities and do not provide information about the global flow field inside the combustion chamber. Therefore, typical flow values like the tumble number or tumble ratio can differ from the results in Fig. 16a. The results of both measurements with the tumble flap (dashed and dash dotted line) may underpin this fact. Both configurations showed slightly decreasing velocities from -50 to -35°CA after TDC. Afterwards both increased again. The authors assumed a local phenomenon and attributed it to an asymmetrical movement of the tumble vortex. However, this local flow information around spark plug and its effects on spark elongation are of immense importance for the combustion process in SI engines.

Similar in the sequence was the result for the calculated turbulence presented in Fig. 16b. At first, the low flow intensity of the VOT125 configuration with the EIVC (dotted line) resulted in almost zero TKE without using the tumble flap. With tumble flap, TKE increased extremely during late compression, especially for the big valve lift profile (dash dotted line).

In general, this investigation showed plausible results and encourage further investigations with VRA as a measurement technique for local in-cylinder flow and turbulence.

5.2 Correlation of TKE and combustion speed

Flow parameters should also result in qualitative good correlations to combustion parameters. Figure 17 demonstrates one approach. Firstly, VRA measurements under motored conditions with different charge motion setups were performed as already discussed in the section before. Secondly, fired operation allowed combustion diagnostics and heat release calculation. For all fired measurements a variation of air fuel ratio λ was done, whereas for the comparisons to flow values a λ of 1.2 was chosen as diluted mixtures showed differences in combustion behaviour between the applied configurations more significant.

From the measured in-cylinder pressure mass fraction burned (MFB) calculation was performed, which is represented by the solid line in Fig. 17. For all measurements the centre of combustion (MFB = 50%) was kept constant at around 8°CA after TDC.

Combustion parameters like MFB 5%, 50% and 95% were derived from the heat release trace. The combustion duration was defined between 5 and 95% MFB. These values defined the section for averaging flow parameters. In the example of Fig. 17 the TKE was averaged between 0 and 20°CA after TDC. Regarding the contents of Fig. 16 it is obvious that the combustion period was always far later than the maximum of TKE. Hence, this showed the immense importance for combustion process to hold up the flow intensity within compression until TDC.

Figure 18 finally shows the result. As one can see, TKE and combustion duration of the four configurations showed a clear correlation. The measurements with the tumble flap (triangle and square) demonstrated the highest TKE and the shortest burning duration. The larger valve lift without tumble flap (dot) showed slightly lower values. For the EIVC without tumble flap (rhombus) the longest burning duration of around 37.5°CA confirmed the VRA measurement, which determined almost no turbulence for this configuration.

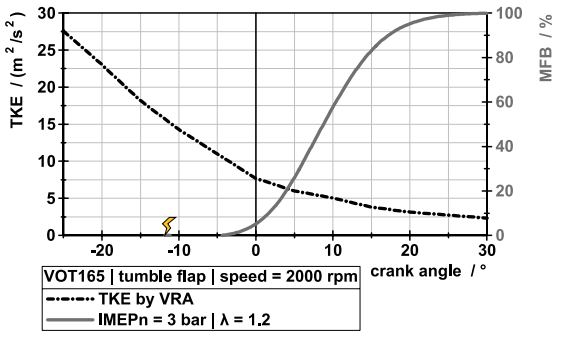

Fig. 17 TKE (dash dotted line) and MFB (solid line) for VOT165 with tumble flap at 2000 rpm; ignition timing at − 12 °CA after TDC

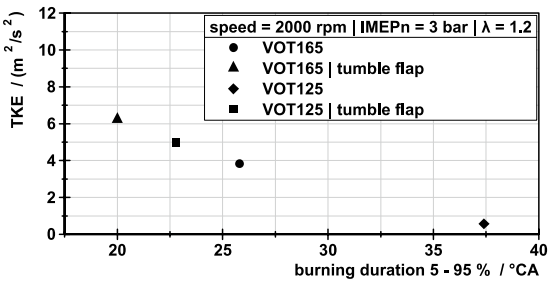

Fig. 18 Correlation of TKE and burning duration of the four different inlet configurations: VOT165 (circle), VOT165 with tumble flap (triangle), VOT125 (rhombus) and VOT125 with tumble flap (square)

6 Conclusion

Voltage rise anemometry was successfully developed, validated and applied as a technique to measure in-cylinder turbulence of SI engines, whereas no changes on the combustion chamber were necessary by this novel approach. Correlations to combustion parameters show qualitatively plausible results.

In a first step, fundamental investigations of spark deflections were carried out in a specific flow test rig. Optical recordings of the elongated plasma channel enlarge the understanding and open the possibility of analysing optical flow velocity. Confirming open literature, different dependencies of the voltage drop across the electrodes are found. Longer plasma channel and higher ambient pressure lead to an increase of voltage, whereas a higher electric current flow shows opposite effects.

For implementing voltage rise anemometry as a measurement technique for in-cylinder turbulence the following aspects were essential in this study: An automated post-processing to detect relevant sections within the voltage and current signals. Furthermore, the validated function, which enables the calculation of flow velocities from measured voltage gradients. For this, mathematical functions from open literature are used basically, whereas calibration factors and exponents were recalculated. Additionally, implementation of fundamental statistics to the evaluation process enables computation of flow parameters of cyclic working engines.

Finally, measurements on an ICE with different charge motion setups were performed. Averaged mean flow and turbulence values around TDC show qualitative good results and approve the developed method. Furthermore, a clear correlation between combustion parameters and TKE calculated from VRA substantiates the measurement technique.

Funding Open Access funding enabled and organized by Projekt DEAL.

References

Brandt M, Hettinger A, Schneider A, Senftleben H, Skowronek T (2017) Extension of Operating Window for Modern Combustion Systems by High Performance Ignition. Springer, Cham, Ignition Systems for Gasoline Engines. https://doi.org/10.1007/978-3-319-45504-4

Fischer J (2004) Einfluss variabler Einlassstroemung auf zyklische Schwankungen bei Benzin-Direkteinspritzung. Dissertation, Universität Karlsruhe. In: Forschungsberichte aus dem Institut für Kolbenmaschinen 5/2004. Logos Verlag, Berlin

Gardiner D, Wang G, Bardon M, LaViolette M, Allan W (2008) An experimental study of spark anemometry for in-cylinder velocity measurements. J Eng Gas Turbines Power. https://doi.org/10.1115/1.2898835

Günther M, Nicklitzsch S, Tröger R, Adolf M (2013) Optimizing the Spark Position While Allowing for the Effect of In-Cylinder Flow. Advanced Ignition Systems for Gasoline Engines. Expert Verlag, Renningen. http://d-nb.info/1027632130

Heywood JB (1988) Internal Combustion Engine Fundamentals. McGraw-Hill, New York

Kim J, Anderson R (1995) Spark anemometry of bulk gas velocity at the plug gap of a firing engine. SAE Trans 104:2256–2266. https://doi.org/10.4271/952459

Küchler A (2017) Hochspannungstechnik, 4th edn. Springer Vieweg, Berlin. https://doi.org/10.1007/978-3-662-54700-7

Lancaster DR (1976) Effects of engine variables on turbulence in a spark-ignition engine. SAE Trans 85:671–688. https://doi.org/10.4271/760159

Lindvall FC (1934) A glow discharge anemometer. Electric Eng 53(7):1068–1073. https://doi.org/10.1109/T-AIEE.1934.5056777

Merker G, Teichmann R (2018) Grundlagen Verbrennungsmotoren, 8th edn. Springer Vieweg, Wiesbaden. https://doi.org/10.1007/978-3-658-19212-9

Ogink R, Babajimopoulos A (2016) Investigating the limits of charge motion and combustion duration in a high-tumble spark-ignited direct-injection engine. SAE Int J Engines 9(4):2129–2141. https://doi.org/10.4271/2016-01-2245

Paa A (2019) Einfluss der Zündung auf die Entflammung hochverdünnter Gemische und das Klopfen. Dissertation, Universität Braunschweig. In: Berichte aus dem ivb 23. Shaker Verlag, Düren. https://doi.org/10.2370/9783844071054

Pashley N, Stone R, Roberts G (2000) Ignition System Measurement Techniques and Correlations for Breakdown and Arc Voltages and Currents. SAE Technical Paper 2000–01–0245. https://doi.org/10.4271/2000-01-0245

Riess M, Benz A, Wöbke M, Sens M (2013) Einlassseitige Ventilhubstrategien zur Turbulenzgenerierung. MTZ–Motortechnische Zeitschrift 74:580–585. https://doi.org/10.1007/s35146-013-0172-9

Sandhu NS, Yu X, Yang Z, Dev S, Purohit D, Ting D, Zheng M (2019) An Investigation of Near-Spark-Plug Flow Field and Its Effect on Spark Behavior. SAE Technical Paper 2019–01–0718. https://doi.org/10.4271/2019-01-0718

Schaudt R, Scheuermann A, Ziegler G (1985) Turbulenz und instationäre Flammenausbreitung. Abschlussbe-richt, Forschungsvorhaben Stiftung Volkswagenwerk. Institut für Physikalische Elektronik, Stuttgart

Scheidt M, Brands C, Lang M, Kratzsch M, Günther M, Elsner N, Spannaus T, Vogler C (2014) Kombinierte Miller- / Atkinson-Strategie für zukünftige Downsizing-Konzepte. In: Liebl J (ed) Internationaler Motorenkongress 2014. Springer Vieweg, Wiesbaden. https://doi.org/10.1007/978-3-658-05016-0_16

Schneider A, Leick P, Hettinger A, Hermann R (2016) Experimental studies on spark stability in an optical combustion vessel under

flowing conditions. In: Liebl J, Beidl C (eds) Internationaler Motorenkongress 2016. Springer Vieweg, Wiesbaden. https://doi.org/10.1007/978-3-658-12918-7_22

Shiraishi T, Teraji A, Moriyoshi Y (2016) The effects of ignition environment and discharge waveform characteristics on spark channel formation and relationship between the discharge parameters and the egr combustion limit. SAE Int J Engines 9(1):171–178. https://doi.org/10.4271/2015-01-1895

Stone R (1999) Introduction to Internal Combustion Engines, 3rd edn. Palgrave Macmillan, London. https://doi.org/10.1007/978-1-349-14916-2

Tilz A, Meyer G, Kiesling C, Pirker G, Salbrechter S, Wimmer A (2019) Design of a test rig for fundamental investigations of spark characteristics. Int J Engine Res 21(8):1412–1425. https://doi.org/10.1177/2F1468087419828943

Zadeh MP, Schmidt H, Atkinson W, Naber W (2019) Spark Mechanism in High Speed Flow. SAE Technical Paper 2019–01–0729. https://doi.org/10.4271/2019-01-0729

Zheng M, Chen G, Tjong J, Li L, Yu S, Yu X, Yang Z (2018) Spark-based Advanced Ignition Control for Future Diluted Gasoline Engines. Ignition Systems for Gasoline Engines. Expert Verlag, Tübingen. http://d-nb.info/1171842007